Emergence of a stress transmission length-scale in transient gels

2002 J. Phys.: Condens. Matter 14 2507

(http://iopscience.iop.org/0953-8984/14/10/303)

INSTITUTE OF PHYSICS PUBLISHING JOURNAL OF PHYSICS: CONDENSED MATTER

J. Phys.: Condens. Matter **14** (2002) 2507–2529 PII: S0953-8984(02)31128-7

Emergence of a stress transmission length-scale in transient gels

R M L Evans and L Starrs[1]

Department of Physics and Astronomy, The University of Edinburgh, Mayfield Road, Edinburgh EH9 3JZ, UK

E-mail: Mike.Evans@physics.org and L.Starrs@bristol.ac.uk

Received 22 November 2001
Published 18 March 2002
Online at stacks.iop.org/JPhysCM/14/2507

Abstract

Following a quench, colloidal systems with strong, short-ranged, attractive interactions can exhibit transient gelation, instead of the classical phase-ordering mechanisms of spinodal decomposition or nucleation. The particles aggregate into a tenuous, system-spanning network, which, for a time, remains robust to mechanical disturbance. Eventually, the network's ability to recover from destructive deformations becomes compromised, and the gel collapses. A detailed experimental study of gel collapse was reported in the preceding, companion article, leaving several open questions regarding the processes involved. We present a theoretical investigation into the factors affecting a gel's lifetime, concentrating in particular on the surprising influence of the size and shape of the container. We construct a model in which solvent dynamics are replaced by a dissipative coupling of the particulate network to a fixed frame and show that, in the absence of zero-frequency elasticity, such a coupling results in a novel class of matter in which stresses cannot propagate beyond a finite distance. We find our prediction of the characteristic length to be in quantitative agreement with the experimental data, and show how its ratio to the dimensions of the container controls the sedimentation. We discuss some aspects of the ageing mechanism, and suggest that a sudden collapse is ultimately due to erosion with positive feedback.

1. Introduction

Transient gelation is a ubiquitous mechanism observed in attractive colloidal systems undergoing phase ordering. The colloidal particles bind reversibly into a network, forming what is termed a *physical* gel, as opposed to a *chemical* gel in which covalent cross-linking occurs. Some time after formation the gel suddenly destabilizes, following which phase

[1] Present address: School of Chemistry, University of Bristol, Cantock's Close, Bristol BS8 1TS, UK.

ordering may proceed along classical lines. The formation of particulate gels has been a topic of much research [1–4], though it remains somewhat enigmatic. To equip the reader with a mental image of such gels, we shall review some of the ideas concerned with their formation in the next section. However, the remainder of this article will focus on their collapse, with a view to understanding some aspects of the experiments reported in the preceding, companion article [5]. We leave many of the observed phenomena [5] to future theoretical investigation, and concentrate on the early stage of collapse. It is at this early stage, we shall argue, that the ultimate destiny of the gel is determined.

The accompanying article [5] details experimental measurements of the lifetime of a transient gel. We do not attempt to calculate a formula for this lifetime since it is determined in part by complex late-stage ageing phenomena beyond the scope of this article (but discussed in section 7). We do, however, attempt to explain the observation that, for some samples but not for others, the gel lifetime is affected by the dimensions of the container. This apparently unremarkable observation will turn out to be crucial to understanding the mechanics and mechanisms of transient gels.

Building on what is known from experimental investigations, as discussed in sections 2 and 3, we construct a coarse-grained theoretical model of gel sedimentation by identifying the relevant macroscopic order parameters as concentration, velocity and stress in the network structure. This model is presented in section 4. Although simple, our model explains some of the settling behaviour observed in transient gels. It also identifies the physical processes involved in gel collapse, thus providing a general framework for the description of transient gelation on which a more detailed model may be constructed. We stress that our theoretical approach is a general one and should be applicable to transient gels formed in any weakly aggregating system.

Using the model we shall show that the principal material properties by which to characterize a gelled system are the bulk viscosity of the network and the coefficient of drag due to solvent back-flow. Dimensionally, the ratio of these quantities defines a length-scale, the ‘stress screening length’, the significance of which will be investigated in detail. We shall show that transient gels belong to a novel class of matter in which transport of momentum, by diffusion or sound propagation, is screened beyond this finite characteristic length-scale. The crux of the physics is this: a mechanical perturbation will cause a distortion to propagate through any material. If the material (in this case, the network of particles) has a finite elastic memory, then the signal must eventually be lost if momentum is non-conserved due to a dissipative background of solvent. The upshot of this is that, for large samples, the majority of the gel cannot ‘feel’ the presence of the boundary walls of its container, so that the suspension falls at its terminal velocity. Smaller samples, or those that can store elastic forces for longer, are able to transmit stresses that substantially alter the system’s behaviour.

Following the presentation of the model, we estimate, in section 5, the values of its parameters by considering the rates of various structural rearrangements. In section 6 we compare the qualitative and quantitative predictions with the results of the experiments reported in the preceding, companion paper [5]. From the experimental data, we determine the stress screening length, and demonstrate agreement with our predictions. Finally we shall discuss the implications of this work in section 7.

2. Gel formation and structure

It has been widely observed that the classical picture of phase-ordering kinetics is insufficient. When a single thermodynamic phase is quenched into a co-existence region of its phase

diagram, it may evolve towards two-phase equilibrium via a number of alternative processes. According to the classical mean-field theory of phase ordering [6], if the initial state is unstable with respect to concentration fluctuations, phase separation will proceed by spinodal decomposition, leading rapidly to a mesoscopic texture of interconnected domains of the separated phases. Alternatively, if formation of an interface between phases carries a price of surface energy, the initial state may be metastable. In this case, an energetically unfavourable (and therefore rare) condensation nucleus must fluctuate into existence before growing into a macroscopic second phase.

A third process, not predicted by the classical theory, has been seen for particularly deep quenches of colloidal systems with short-ranged attractive interactions [1, 2]. The particles assemble into a tenuous, system-spanning network with a structure that is locally fractal [1], giving the system the properties of a gel. It has been shown that particulate gels resulting from the deepest quenches into the equilibrium two-phase region (with inter-particle attractions many times k_BT) have the features of diffusion-limited cluster–cluster aggregation (DLCA), both in the form of the static structure factor $S(q)$ [1] and in the time dependence of its peak $q_m \sim t^{-1/d_f}$ during formation [2] (where d_f is the local fractal dimension). The canonical DLCA algorithm [7] cannot reproduce the transient nature of a gel, unless modified to allow random breaking and reformation of bonds [8]. In simulations, this reversible DLCA was shown to exhibit a lower limit on the concentration for which system-spanning clusters form [8], in qualitative agreement with the existence of a 'gel line' in the phase diagram. Clearly, the canonical DLCA represents one limit of the modified process, as bond lifetime, or equivalently attraction strength, tends to infinity. For weaker bonds, or low particle concentrations, the structures formed become, to the eye at least, more akin to spinodal textures. However, the local structure is fractal rather than liquid-like [8]. In experiments too, the behaviour of some gels hints at spinodal decomposition. For fairly shallow quenches, still in the gel region, the peak in the structure factor evolves as $t^{-1/3}$ [2], although local structure is still fractal. The crossover from DLCA-like to spinodal-like behaviour continues for attraction strengths *below* the gel line, where a non-percolating liquid phase with a strangely fractal structure has been observed to form, in two dimensions, by spinodal dynamics [9].

The significance of the fact that this transient gelation has been observed in colloidal systems, as opposed to atomic or molecular ones, may be only that length- and timescales of colloidal phase ordering are sufficiently large to be easily observable. Whatever the description of the formation process, the transient gels all seem to share two features: non-ergodicity and percolation. Recent measurements of the dynamic structure factor in transient gels [3] suggest glassy properties, despite rather low particle concentrations ($\phi \sim 0.2$) not usually associated with structural glasses. The measurements revealed correlations whose decay is very slow, and appears to depend on the age of the system, indicating glassy non-ergodicity. This is in broad agreement with recent mode-coupling theory (MCT) calculations for hard spheres with short attractive interactions [10]. The MCT predicted a non-ergodicity transition, close to the experimental gel line, at which relaxations are impeded by local bond formation [10]. The importance of percolation was discovered in recent simulations of Brownian hard spheres with short, attractive interactions [4], for which the large-scale structure, inaccessible to MCT, was analysed. In the simulations, the measurement of sub-diffusive particle transport, indicating non-ergodicity, was taken to indicate the formation of a gel. The percolation threshold was plotted and found to pass continuously across the stable fluid boundary into the two-phase region(s). This threshold was estimated to be the transient gelation threshold [4], although the gel line obtained by experiment is observed at higher concentrations [2].

3. Gel collapse

Colloidal gels are transient in nature, and therefore eventually destabilize. For the case where the density of particles is greater than that of the suspending solvent, the destabilization of a gel is marked by a sharp increase in its sedimentation rate by one or two orders of magnitude [3]. This settling behaviour, known as delayed sedimentation, has been observed in many weakly attractive systems [11–13] but it remains a poorly understood phenomenon.

The detailed observations of collapsing gels reported in the accompanying article [5], as well as some previous studies [3, 14], have shown a wide range of features, indicating great physical richness. In the experiments [3,5,14], a colloidal suspension of near-hard spheres was induced to gel by adding random-coil polymer to the solvent, causing an effective attraction between the colloidal spheres via the depletion mechanism [15]. Once these mixtures had been homogenized by tumbling, and then left to gel, the subsequent sedimentation of the gelled suspension was observed to follow a number of different courses. For strong inter-particle attractions $\sim 10 k_B T$ (induced by a high concentration of added polymer), sedimentation occurred at a low but fairly uniform rate. With weaker attractive interactions ($\sim$4–$8 k_B T$), the gels were initially slow to sediment, continuing almost to fill the container for several hours before suddenly collapsing to a much smaller volume over a period of about 1 h, settling as a dense sediment. Thus, these colloid–polymer gels exhibited 'delayed sedimentation' with a lifetime (time before the onset of the rapid collapse) which could be well defined. The gels with a definite lifetime were further sub-categorized [14], as it was noticed that the lifetime could depend on the initial height of the sample and even on the shape of the container. However, gels with particularly weak inter-particle attractions were not observed to exhibited such geometrical dependence [3, 14]. A more exhaustive study [5] has demonstrated that, where height dependence is evident, it eventually saturates given a sufficiently tall sample. Similarly, the accompanying experimental study [5] reveals a dependence of the lifetime on sample width, that is found to saturate for a sufficiently wide geometry. The data from this study [5] are discussed further in section 6.

Before proceeding to the next section, let us briefly consider the question 'why does a transient gel collapse?'. Clearly, since crystal–fluid coexistence is the equilibrium state of the system, the gel would not be expected to last indefinitely. However, this does not explain the mechanism of its demise. To solve the mystery, one might endeavour to identify some cause of breakage of the system-spanning network[2]. Paradoxically, this would not provide an explanation for the collapse, since the gel is apparently indifferent to the breakage of its structure, as witnessed by several experiments. In one such experiment [14], a steel ball, several millimetres in diameter, was introduced into a freshly gelled sample, and moved through the gel by a hand-held magnet. This abuse of the delicate networked structure did not measurably alter the gel's lifetime. Furthermore, at low shear rate, a large shear deformation ($\gg 100\%$) affected by a rheometer does not precipitate collapse [3], although the gel's system spanning structure must be broken many times over by such treatment. Also, a freshly formed gel may be poured from one vessel to another without ill effect. Indeed, the most brutal treatment of a gel; to shake it until all particles are torn from the aggregate and dispersed homogeneously; is precisely the method of preparing a sample for gel formation. Clearly then, the structure of a fresh gel can sustain continued breakage, since it has the ability to re-connect or heal itself. So gel collapse must indicate that this healing ability has been compromised. These ideas will be further quantified in the discussion of microscopic rates in section 5 and of ageing in section 7.

[2] Such an explanation is mooted in [16].

4. Continuum model of a sedimenting gel

To understand the influence of large-scale geometry on a gel, we now develop a continuum picture of force balance within a sedimenting sample. The general equations of motion are determined in section 4.1, and solved in Fourier space to yield a dispersion relation, in section 4.2, which we shall interpret in real space. Using some general results from that investigation, we develop a simplified model of sedimentation in various specific geometries in sections 4.3–4.5.

4.1. Equations of motion

A gel is an inter-connected network of colloidal particles immersed in a solvent at low Reynolds number. The particles are generally not neutrally buoyant in the solvent, hence the eventual sedimentation. Let us consider the forces experienced by a small (but sufficiently large to be regarded as homogeneous) element of the network. It feels a tensorial stress $\boldsymbol{\sigma}$ transmitted by neighbouring elements, and a force $\boldsymbol{f}$ (per unit volume) due to external fields including gravity. An element of the particle network also experiences a drag force from the solvent through which it passes, proportional and opposite to its velocity $\boldsymbol{v}$ relative to the fixed frame of the container. The constant of proportionality Γ depends on the viscosity of the solvent and the geometry of channels through which it must pass between aggregated particles. This description may be regarded as a special limit of a two-fluid model [16], in which the 'fluids' are the solvent and the particle network. One of the fluids (the solvent) is incompressible and of much lower viscosity than the other. Additionally, the solvent has no large-scale hydrodynamics, as its flow is screened by the porous nature of the aggregate. Hence solvent back-flow is an entirely local phenomenon, and all the solvent's hydrodynamics are embodied in the term $\Gamma\boldsymbol{v}$.

If the particle network has a mass density ρ, exclusive of the suspending solvent, then applying these forces to Newton's second law gives

$$\rho\dot{\boldsymbol{v}} + \Gamma\boldsymbol{v} + \nabla\cdot\boldsymbol{\sigma} = \boldsymbol{f} \tag{1}$$

where the tensor of stress transmitted through the network has been contracted with a gradient operator to yield the unbalanced force on an infinitesimal element $\nabla_\beta\sigma_{\alpha\beta}$.

We require a constitutive relation to prescribe the network stress $\boldsymbol{\sigma}$. To preserve as much generality as possible, let us make only one assumption: that the constitutive relation is linear. We assume, for the moment, that such a linear response regime exists. Later, we shall consider the effects of non-linearity. The relation between a shear stress and strain rate in a viscoelastic substance is routinely expressed in terms of the time-dependent stress relaxation modulus or memory function $G(t)$. The tensorial generalization of this, to encompass stresses and strains other than simple shear, is

$$\boldsymbol{\sigma}(t) = -\int_{-\infty}^{t} \mathrm{d}t'\ \boldsymbol{G}(t-t') : \nabla\boldsymbol{v}(t') \tag{2}$$

where the tensor gradient of velocity $-\nabla\boldsymbol{v}$ is the generalization of simple shear rate. The fourth-rank tensor $\boldsymbol{G}(t)$ has components $G_{\alpha\beta\gamma\delta}$ that determine the force component induced in direction α across a surface in direction β by the gradient which occurred in direction γ of the velocity component in direction δ at some earlier time. Rather than writing equation (2) in an explicitly symmetrized form (with $\nabla\boldsymbol{v}$ replaced by $\nabla\boldsymbol{v} + (\nabla\boldsymbol{v})^T$), we have chosen a compact notation by absorbing this symmetrization into the definition of $\boldsymbol{G}$.

Strictly speaking, the quantity $\boldsymbol{\sigma}$ appearing in the equation of motion (equation (1)) is the Eulerian stress field, which is the force across a unit area at a fixed point. On the other hand, equation (2) gives the Lagrangian stress, which is the force across a surface that is fixed

relative to the gel. The time integral should not be evaluated at a fixed point in space, but rather for a fixed element of the gel, since the stress in a given gel element is determined by its own history, not by the history of the spatial point at which it presently resides. Such subtleties can be ignored if displacements are either small in amplitude, or take place on a timescale longer that the material memory for which $\boldsymbol{G}(\tau) \to 0$. In the former case gel elements remain identified with a fixed point in space, and in the latter elements forget that they have not always lived in the same place.

Note that the stress relaxation modulus $\boldsymbol{G}(t)$ appearing in equation (2) is not the one that would be measured in a rheometric experiment. Rheometry measures the response of the whole system: particle network plus solvent. Equation (2) gives the part of the stress carried only by the network. This stress is measured only in a hypothetical experiment where a force can be applied on the network alone, with the solvent replaced by a frictionless fluid or a vacuum.

4.2. Momentum transport

Let us now solve the equations of motion (equations (1) and (2)) to find how a generic perturbation propagates through the system. We define the temporal Fourier transform of the velocity field by

$$\boldsymbol{v}(\boldsymbol{r}, t) = \int_{-\infty}^{\infty} \tilde{\boldsymbol{v}}(\boldsymbol{r}, \omega) \mathrm{e}^{\mathrm{i}\omega t} \, \mathrm{d}\omega \tag{3}$$

with $\tilde{\boldsymbol{v}}(-\omega) = \tilde{\boldsymbol{v}}^*(\omega)$ to ensure a real velocity field, and similarly for the external force $\boldsymbol{f}$. Substituting into equations (1) and (2) yields

$$\nabla \cdot \boldsymbol{G}^*(\omega) : \nabla \tilde{\boldsymbol{v}} + (\omega^2 \rho - \mathrm{i}\omega\Gamma)\tilde{\boldsymbol{v}} = -\mathrm{i}\omega \tilde{\boldsymbol{f}}(\boldsymbol{r}, \omega) \tag{4}$$

in terms of the complex viscoelastic modulus tensor

$$\boldsymbol{G}^*(\omega) \equiv \mathrm{i}\omega \int_0^{\infty} \boldsymbol{G}(\tau) \mathrm{e}^{-\mathrm{i}\omega\tau} \, \mathrm{d}\tau. \tag{5}$$

In the inhomogeneous equation (4), the external force $\boldsymbol{f}$ acts as a source of perturbations, i.e. gravity and boundaries displace the network. The system's response, i.e. the way in which a perturbation propagates, is determined by the auxiliary equation ((4) with $\boldsymbol{f} = \boldsymbol{0}$), which is solved by linear combinations of functions of the form

$$\tilde{\boldsymbol{v}}(\boldsymbol{r}, \omega) = \hat{\boldsymbol{v}}(\omega) \mathrm{e}^{\mathrm{i}\boldsymbol{k}\cdot\boldsymbol{r}} + \hat{\boldsymbol{v}}^*(\omega) \mathrm{e}^{-\mathrm{i}\boldsymbol{k}\cdot\boldsymbol{r}}. \tag{6}$$

Substituting this into equation (4) with $\boldsymbol{f} = \boldsymbol{0}$ leads to the condition

$$G^*_{\alpha\beta\gamma\delta}(\omega) \, k_\beta \, k_\gamma \hat{v}_\delta(\omega) = (\omega^2 \rho - \mathrm{i}\omega\Gamma)\hat{v}_\alpha(\omega). \tag{7}$$

We may choose, without loss of generality, to orient one coordinate axis along the wave direction $\boldsymbol{k}$, so that $\boldsymbol{k} = (0, 0, k)$. Then equation (7) simplifies to

$$G^*_{\alpha k k \delta} \hat{v}_\delta = \left(\frac{\omega^2 \rho - \mathrm{i}\omega\Gamma}{k^2} \right) \hat{v}_\alpha \tag{8}$$

(summing on Greek indices only), which is an eigenvector equation for the second-rank matrix $G^*_{\alpha k k \delta}(\omega)$. In three dimensions there are three solutions, with different orientations of the velocity vector $\hat{\boldsymbol{v}}$ relative to the wavevector $\boldsymbol{k}$. For simple materials these would be one longitudinal and two transverse modes of momentum propagation, although for complex materials with a skew tensor modulus the eigenvectors may point in other directions. Each of the three modes has an associated eigenvalue $G^*(\omega)$ corresponding, for example, to shear and bulk moduli for simple materials. Identifying this eigenvalue with the coefficient in

equation (8) yields the value of k in terms of ω. Expressing each eigenvalue in terms of its real and imaginary parts, the storage and loss moduli $G^* \equiv G' + \mathrm{i}G''$, the dispersion relation for any of the three modes becomes

$$k^2 = \frac{\omega^2\rho - \mathrm{i}\omega\Gamma}{G'(\omega) + \mathrm{i}G''(\omega)}. \tag{9}$$

The dispersion relation is a Fourier-space constraint on perturbations to the gel. Let us consider its implications for the motion in real space. The above derivation has followed very standard lines for the solution of the equations of motion of a generic material. Consequently, the expected behaviour of familiar materials is embodied in certain limits of the dispersion relation (equation (9)). Additionally, for realistic parameters corresponding to a colloidal gel, the relation reveals some interesting properties.

Clearly the wavevectors given by equation (9) are complex, $k \equiv k' + \mathrm{i}k''$. In the context of equation (6), the reciprocal of the imaginary part, k''^{-1}, is a decay length. That is to say, a wave of frequency ω will decay over a distance k''^{-1}. Let us first consider the case of no losses from dissipative coupling to the solvent ($\Gamma = 0$). This is the usual situation, since materials are normally expected to respect Galilean invariance, and therefore cannot notice absolute velocity as appears in the second term of equation (1), but feel only velocity gradients.

With the Galilean condition ($\Gamma = 0$), if the network is purely elastic ($G'' = 0$) then the dispersion relation is entirely real, so the decay length k''^{-1} is infinite since there are no losses. In this pedagogically familiar case, $k^2 \propto \omega^2$ so sound propagates, with a phase velocity $\sqrt{G'(\omega)/\rho}$. Real materials, on the other hand, are lossy ($G'' \neq 0$) so k'' (and consequently the decay length) is finite at finite frequency. However, the right-hand side of equation (9) vanishes in the low-frequency limit so the decay length k''^{-1} diverges, and momentum is transported across the system. This is the case for an elastic solid, where $G'(0)$ is finite so $k^2 \overset{\sim}{\to} \omega^2$ and low-frequency sound propagates. It is also the case for a material with zero yield stress ($G'(0) = 0$). Classically, for such a material, $G''(\omega) \to \omega\eta$, where η is static viscosity, so that low-frequency momentum transport is by diffusion ($k^2 \sim \omega$). G'' can vanish non-linearly with ω, but always more slowly than ω^2, so that $k''^{-1} \to \infty$.

If Galilean invariance is broken by a dissipative coupling to a fixed frame ($\Gamma \neq 0$), however small, the situation is quite different. In this case, an elastic solid ($G'(0) \neq 0$) is still able to transport momentum across the system ($k''^{-1} \to \infty$) at low frequency, but it is now a diffusive process, since $k^2 \to -\mathrm{i}\omega\Gamma/G'(0)$ as $\omega \to 0$. With no static elasticity, and a viscous low-frequency modulus $G''(\omega) \to \omega\eta$, there is no frequency at which $k''^{-1} \to \infty$. The maximum decay length is at $\omega = 0$, where $k''^{-1} = r_0 \equiv \sqrt{(\eta/\Gamma)}$. Hence momentum is not transported across this system. Instead, velocity perturbations are exponentially screened beyond a distance r_0. Some materials have non-trivial low-frequency viscoelastic response, with $G''(\omega)$ varying as a power of ω. If this power is less than unity, the viscosity $\eta \equiv \lim_{\omega\to 0} G''(\omega)/\mathrm{i}\omega$ diverges, as does r_0, and momentum is transported to infinity sub-diffusively. With a power greater than unity, the decay length will have a maximum (defining the screening length r_0) at a non-zero frequency.

The screening of momentum that has arisen here should not be confused with the well known screening of solvent flow through static porous media. That screening was mentioned in section 4.1, and is the reason that the hydrodynamics of solvent back-flow can be treated locally. In the present case, it is the porous medium itself (the particle network) whose momentum is screened, given certain criteria. As the viscosity of the network increases, so does the screening length r_0, while the penetration depth for perturbations of the solvent flow field depends only on the 'pore' size.

In summary, materials with zero yield stress, non-diverging viscosity and a dissipative coupling to a fixed frame are in a distinct and unusual class, for which momentum transport is exponentially screened beyond a length-scale characteristic of the material. Every other class of matter can transport momentum to infinity via sound, diffusion or anomalous diffusion. We shall argue that the resulting novel class of matter with screened momentum transport includes some transient particulate gels. If the inter-particle attractions are relatively weak then, on the longest timescales, thermal motion must cause the memory function $\boldsymbol{G}(t)$ of such a gel to decay, so that its low-frequency viscoelastic modulus is purely dissipative. The resulting structural viscosity will be quantified in section 5. For the present we assert that, for the transient gels in question, $G'(\omega) \to 0$ as $\omega \to 0$ so that they possess a stress screening length. Of course, the solvent in which the aggregated network is suspended can transmit sound, in order to carry information about the rest-frame of the container. However, in order to view the particle network as a material distinct from the solvent, we have implicitly assumed that the speed of sound in the solvent is effectively infinite in comparison with the processes of interest.

The existence of a screening length $r_0 = \sqrt{(\eta/\Gamma)}$ (in fact, three screening lengths: one for each low-frequency normal mode) may explain some of the experimental observations of transient gels. One might expect the network viscosity η to be an increasing function of inter-particle attraction strength (as we shall estimate in section 5). Certainly this is observably true of the *rheometric* shear viscosity [14] (a property of the whole system, including solvent). If so, then gels with the weakest inter-particle attractions have the shortest screening length r_0. If the dimensions of a gel sample are greater than r_0, then network stresses cannot be transmitted across the system. In particular, if the sample is taller than r_0 then the top of the aggregated network cannot feel a supporting force transmitted from the bottom of the container. If the top surface of the gel cannot receive a signal from the bottom of the container, and is therefore unaware of its existence, then no properties of the sample can be a function of its height. This could explain why gel lifetimes were observed to become independent of the sample height for particularly weak inter-particle attractions [14].

4.3. Sedimentation

The emergence, from the dispersion relation, of a decay length which is maximum at zero frequency is useful in constructing a model of gel sedimentation. It reveals that the most important parameters governing the large-scale behaviour of a gel are the drag coefficient Γ and the three zero-frequency viscosities η. Hence a minimal model using only these parameters should capture the principal macroscopic features of the physics, without the need for a more detailed description of $G^*(\omega)$. Such a model is now investigated.

To model a gelled sample in the early stage of sedimentation at a steady rate, only one spatial direction is non-trivial if we ignore the effects of wall friction (which we shall consider in the following sections). Let us imagine a semi-infinite sample, bounded only by the base (at $z = 0$) of an infinitely broad container. In this case, equation (1) reduces to a scalar equation. With the justification given above, we replace the network's stress relaxation modulus in equation (2) by its low-frequency limit, which we assume (as argued in section 5) is viscous, $G_{zzzz}(t) \to \eta_c\,\delta(t)$. Hence the network reacts against compression with a stress proportional to the rate of compression, and η_c is a compressional viscosity. The external force density f in equation (1) is due to gravity g acting on the suspended particles, which are not neutrally buoyant. Their mass density differs from that of the solvent by $\Delta\rho$. If ϕ is the concentration (volume fraction) of the colloidal particles, then $f = -\Delta\rho g\phi(z, t)$ with the positive z direction defined vertically upwards. Hence, in the over-damped limit ($\Gamma v \gg \rho\dot{v}$) the equation of motion (equation (1)) becomes

$$\Delta\rho g\phi = \eta_c \frac{\partial^2 v}{\partial z^2} - \Gamma v \tag{10}$$

which states that the non-buoyant weight of colloidal particles is supported both by stress transmitted through the viscous network, and by drag due to solvent back-flow.

In the absence of structural support ($\partial^2 v/\partial z^2 = 0$), sedimentation is at the ϕ-dependent terminal velocity which, for the initial concentration ϕ_0, is $v = -v_0$, given by equation (10) as $v_0 = \Delta\rho g\phi_0/\Gamma$. So equation (10) can be re-written as

$$\left(\frac{\partial}{\partial z/r_c}\right)^2 \frac{v}{v_0} - \frac{v}{v_0} - \frac{\phi}{\phi_0} = 0 \tag{11}$$

where the compressional stress screening length $r_c = \sqrt{(\eta_c/\Gamma)}$ has emerged.

Having introduced a new dynamical variable $\phi(z, t)$, we require an extra constraint for closure, which is supplied by continuity:

$$\frac{\partial\phi}{\partial t} = -\frac{\partial(v\phi)}{\partial z}. \tag{12}$$

A steady-state solution exists for equations (11) and (12), given by setting $\partial\phi/\partial t = 0$ with boundary conditions $v(0) = 0$ and $\phi(\infty) = \phi_0$. However, this solution is unphysical, as it requires a constant material flux into the boundary at $z = 0$, but no flux out, so that the concentration ϕ becomes infinite here. This is a result of choosing a linear constitutive relation. In practice, the response to compression cannot remain linear for arbitrarily large amplitudes since, beyond a certain concentration, a sediment strongly resists further compaction. This non-linearity is easily incorporated into our model if we demand that the sedimentation velocity v falls to zero at a given concentration ϕ_s, which is the concentration of the dense sediment observed experimentally. As this dense sediment builds up, its top surface must rise at a speed v_s, given by $(\phi_s - \phi_0)v_s = \phi_0 v_0$, due to conservation of matter.

The equations of motion have a physically realistic steady state in the rest frame of the sediment surface. Transforming to a spatial coordinate $\zeta = z - v_s t$ (so that $(\partial/\partial t)_z = (\partial/\partial t)_\zeta - v_s(\partial/\partial\zeta)_t$), and demanding $(\partial/\partial t)_\zeta = 0$ in equation (12) yields

$$\frac{\phi}{\phi_0} = \left[\frac{\phi_0}{\phi_s} - \left(1 - \frac{\phi_0}{\phi_s}\right)\frac{v}{v_0}\right]^{-1} \tag{13}$$

which is substituted into equation (11) with $\partial^2/\partial z^2 \to \partial^2/\partial\zeta^2$ and boundary conditions $v(0) = 0$, $v(\infty) = -v_0$. This ordinary differential equation was solved by a numerical relaxation method for various values of the parameter ϕ_0/ϕ_s. Results for the concentration ϕ and speed $|v|$ are plotted in figure 1, as a function of height above the sediment in units of the characteristic length r_c. In each case, the gel at large heights remains at its initial concentration ϕ_0 and settles at its terminal velocity, supported only by drag. Conversely, near the dense sediment, and up to a height of order the stress screening length r_c, the gel is compressed and decelerated.

We expect such a steady state to be achieved in samples whose initial height is much greater than their characteristic length r_c. If this is not the case, then the profile throughout the sample will evolve with time, and depend on the initial height. To model that situation (which we shall not pursue here) would require a no-stress boundary condition at the (descending) top surface of the gel.

4.4. Sedimentation between walls

Having modelled sedimentation toward the base of a tall container, and far from its walls, let us now consider a steady state in another geometry. At a height $z \gg r_c$, where the influence

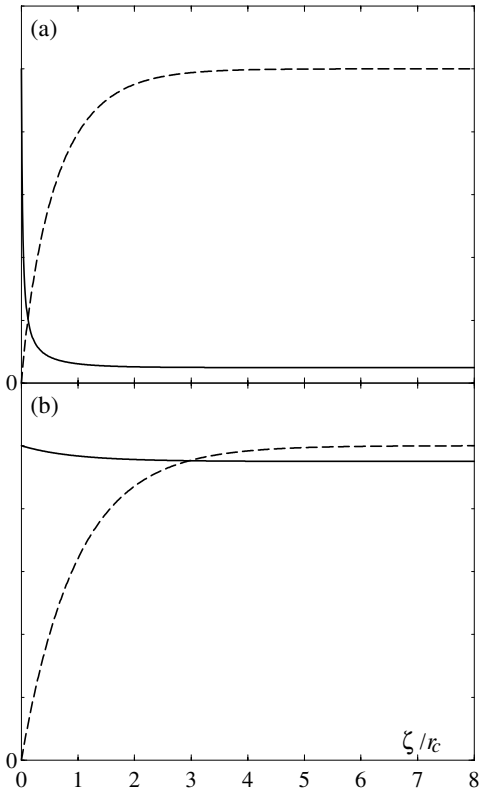

Figure 1. Steady-state speed $|v|$ (dashed curves) and concentration ϕ (solid curves), in arbitrary units, as a function of height ζ above the advancing surface of dense sediment, in units of the stress screening length r_c. Ratio of initial concentration ϕ_0 to sediment concentration ϕ_s is (*a*) 5%, (*b*) 95%.

of the base is not felt, we can find the sedimentation velocity as a function of distance x across a sample of width L_x, with plane vertical walls at $x = \pm L_x/2$. We assume that the other horizontal dimension L_y is large, so that no other boundaries influence the motion, and the walls at $x = \pm L_x/2$ are effectively infinite planes.

In this case, the only non-zero component of velocity is v_z, and of gradient is $\nabla_x v$, so that, in the limit of over-damping ($\rho\dot{v} \ll \Gamma v$) and low frequency where $G_{zxxz}(t) \to \eta_s\delta(t)$, equations (1), (2) yield

$$r_s^2 \frac{\mathrm{d}^2}{\mathrm{d}x^2}\frac{|v|}{v_0} - \frac{|v|}{v_0} + 1 = 0 \tag{14}$$

where we have used the fact that the velocity field has no divergence, so that the concentration remains at ϕ_0. Here, η_s is the shear viscosity, and $r_s \equiv \sqrt{(\eta_s/\Gamma)}$ is the shear stress screening length. With the boundary conditions $v = 0$ at $x = \pm L_x/2$, equation (14) is solved by

$$\frac{|v|}{v_0} = 1 - \frac{\cosh(x/r_s)}{\cosh(L_x/2r_s)}. \tag{15}$$

In the limit $\eta_s \ll \Gamma$ (so $r_s \to 0$), sedimentation is uniform at the terminal velocity $|v|/v_0 \to 1$. For r_s finite but small compared with L_x, equation (15) describes plug flow, with $|v| \approx v_0$ far from the walls while, near each wall, a layer of thickness $\sim r_s$ undergoes shear.

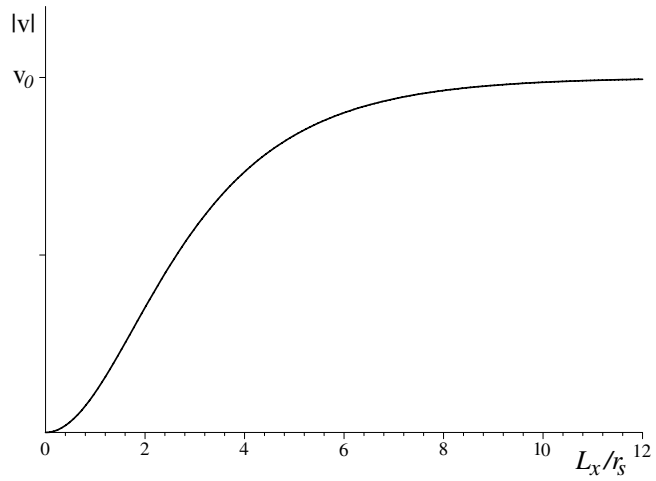

Figure 2. Sedimentation speed $|v|$ on the centre-line ($x = 0$) as a function of container width L_x in units of the shear stress screening length r_s, for steady sedimentation between two parallel walls.

In the opposite limit, where $\eta_s \gg \Gamma L_x^2$ (so the stress screening length exceeds the sample size), equation (15) becomes independent of Γ, and describes a Poiseuille-like parabolic flow profile

$$|v| \to \frac{v_p}{8}\left[1 - \left(\frac{2x}{L_x}\right)^2\right] \tag{16}$$

with

$$v_p \equiv \frac{\Delta\rho g \phi_0 L_x^2}{\eta_s} = \left(\frac{L_x}{r_s}\right)^2 v_0. \tag{17}$$

In figure 2, the speed of sedimentation on the centre-line $x = 0$ is plotted, from equation (15), as a function of the width L_x of the container. Clearly, for $L_x \gg r_s$ the velocity is terminal and independent of the container's width, while for $L_x \ll r_s$ forces from the walls retard the sedimentation. It is noticeable that the speed remains strongly width dependent up to $L_x \sim 4r_s$.

4.5. Sedimentation in a finite container

Finally, let us consider sedimentation in the geometry of a real container, bounded in all three dimensions (once more in the over-damped limit $\Gamma v \gg \rho \dot{v}$). A general solution in this case is rather involved, but interesting physics may be learnt from studying the form of the governing equations of motion. We assume that velocity is always oriented in the z-direction, but now allow gradients in all directions. As before, we take the low-frequency limit and assume a non-skew modulus, so that $G_{z\beta\gamma z}(t) = \eta\delta_{\beta\gamma}(t)$ with the compressional viscosity $\eta = \eta_c$ for $\beta = z$, and the shear viscosity η_s otherwise. Hence, equations (1) and (2) yield the partial differential equation

$$\left(\frac{\partial}{\partial x/r_s}\right)^2 \frac{v}{v_0} + \left(\frac{\partial}{\partial y/r_s}\right)^2 \frac{v}{v_0} + \left(\frac{\partial}{\partial z/r_c}\right)^2 \frac{v}{v_0} - \frac{v}{v_0} = \frac{\phi}{\phi_0}. \tag{18}$$

Since ϕ_0 is the initial concentration, the right-hand side of equation (18) is typically of order unity. If v is typically of order the terminal velocity v_0, as it is in a large container, then it is

clear from equation (18) that variations in velocity are typically on length-scales of order the stress screening length (for shear r_s in x and y directions, and for compression r_c in z).

If, on the other hand, one dimension of the container (L_x, say) is much smaller than the relevant characteristic length (r_s), then the typical velocity scale is no longer v_0, but v_p as shown in section 4.4. Using the definition $v_p \equiv v_0(L_x/r_s)^2$, equation (18) can be re-cast as

$$\left(\frac{\partial}{\partial x/L_x}\right)^2 \frac{v}{v_p} + \left(\frac{\partial}{\partial y/L_x}\right)^2 \frac{v}{v_p} + \left(\frac{\eta_c}{\eta_s}\right)^2 \left(\frac{\partial}{\partial z/L_x}\right)^2 \frac{v}{v_p} = \frac{\phi}{\phi_0} + \left(\frac{L_x}{r_s}\right)^2 \frac{v}{v_p}. \tag{19}$$

Here, the last term is negligible if the thickness of the container is small compared with the stress screening length, i.e. $L_x \ll r_s$. In this case, it is immediately apparent from equation (19) that the characteristic scale for variation in any direction is no longer the stress screening length, but the smallest dimension of the container[3] L_x. Hence the condition for a gel's properties to be independent of its initial height L_z (since the top surface cannot feel the presence of the base) is less rigorous than $L_z \gg r_c \equiv \sqrt{(\eta_c/\Gamma)}$, although this condition is sufficient. Height dependence also asymptotes if $L_x \ll r_s$ with $L_z \gg L_x\,\eta_c/\eta_s$.

In practice, as we shall discuss in section 7, steady states such as those modelled here can only be quasi-steady, since the parameters characterizing the sample (η, Γ) must evolve slowly with time as the gel ages. We estimate the early values of these parameters in section 5. Nevertheless, we note some similarity between the concentration profiles in figure 1, and those obtained experimentally for weak gels in the preceding article [5], albeit in the later stages when hydrodynamics and ageing have become complex. The experimental data exhibit a rise in concentration above a dense sediment, over a height interval which may be set by the thickness L_x of the sample cell, and asymptote to a uniform concentration, equal to the initial value. By contrast, experimental concentration profiles for stronger gels vary with time over the entire sample height [5].

5. Estimation of material parameters

As discussed in sections 1 and 2, we have the view of a gelled suspension as a tenuous network of aggregated particles. In the limit of strong, short-ranged inter-particle attractions, the structure is expected to be somewhat like that produced by DLCA. It has been noted by various authors [17, 18] that the rigid, inflexible bonds defining the DLCA process are not appropriate to spherical particles with central potentials, which have no angular rigidity. On contact, attractive hard spheres may bond strongly, but are still free to roll over one another, so that local compaction occurs, and more bonds are formed. Once a sphere has rolled over its neighbours and formed new bonds, to the point that it belongs to a tetrahedral structure, it has no more angular freedom. So a locally compact structure, built from tetrahedral assemblies of spheres, does have the angular rigidity required by DLCA, and can thus aggregate into tenuous clusters on larger length-scales [17, 18]. Hence, the system-spanning network is compact on the scale of a couple of particle diameters, but tenuous (we shall assume self-similarity with fractal dimension d_f), at larger distances, up to the characteristic 'cluster size' ξ, identified in small-angle light scattering experiments [1]. Beyond this scale, clusters cannot continue to be fractal, as a fractal has an ever-decreasing mass density with increasing size. Hence the tenuous clusters are compactly arranged in a space-filling network.

Each cluster has many delicate limbs. Just a few of these limbs are connected to neighbouring clusters, and transmit stress, holding the network together. Those limbs that

[3] $L_x\eta_c/\eta_s$ for the z direction. However, it will be argued, in section 5, that the shear and compressional structural viscosities are approximately equal.

are networked can be said to form the 'backbone' of a cluster, which is a contorted object with fractal dimension d_b. We shall assume that such a backbone behaves as a Hookeian spring, with elastic constant k_e.

We recall from section 3 that the network of particles is in a constant state of breakage and healing. The mechanical response of the network, which we intend to estimate, is dictated by the properties of the connected backbones which transmit stress: their rates of formation and breakage, spring constant and number density. We now proceed to make order-of-magnitude estimates of these quantities, as well as the solvent drag coefficient, which depends on the geometry of the whole aggregate.

5.1. Drag coefficient

The force density due to the flow of solvent, at low Reynolds number, through the particle network, is related to the sedimentation speed v in equation (1) via the drag coefficient Γ. In the reference frame of the sedimenting particle network, v is the macroscopic rate of flow of solvent. Regarding the network as a porous medium, Darcy's law [19, 20] states that, at low Reynolds number, this flow rate is proportional to the pressure gradient (equivalent to force density), with constant of proportionality k/μ, which defines the 'permeability' k. Hence our drag coefficient is the ratio of solvent viscosity to network permeability. Several methods exist [21] for estimating permeability without explicitly solving the equations of fluid flow in the porous geometry, the simplest of which is the Carman–Kozeny equation [22], which is known to yield good order-of-magnitude estimates for many porous media [20, 21],

$$k \sim \frac{1-\phi}{c_0}\left(\frac{1-\phi}{S}\right)^2. \tag{20}$$

Here, S is surface area per unit volume, and c_0 is a number of order unity. For rough surfaces, such as that presented to the solvent by the aggregated spheres, the specific surface area S is ill defined, as it depends on the resolution of coarse-graining in describing the surface. In the extreme, for a fractal surface, S can diverge, while permeability k remains finite [20]. We find further shortcomings of equation (20), in two specific cases for which all quantities are exactly calculable: a polydisperse set of pipes, and a polydisperse set of parallel-sided cavities. In each case, while equation (20) holds for narrow distributions, it uses the wrong moments of the distribution of sizes of channels, and must therefore fail for high polydispersity. We circumvent both these problems by noting that the quantity in parentheses in equation (20) is a characteristic length, for which we substitute an alternative measure. In determining the fluid velocity at a given point, it is a knowledge of the distance to the nearest obstacle R that is most important, rather than the amount of surface S. We shall term this the remoteness of the point. Its mean square over all space unoccupied by particles, $\langle R^2\rangle_{\text{empty}}$, remains well defined even when the surface is fractal. Moreover, we find that replacing the parenthesized part of equation (20) by $\langle R^2\rangle_{\text{empty}}$ yields an expression for k that employs the correct moments of the distribution of channels for the two polydisperse paradigms (pipes and cavities). The coefficient c_0 then varies little between the two geometries (4/3 for pipes, 2 for cavities). The distribution of remoteness has been measured for simulated DLCA aggregates [23]. If the remoteness is defined to be zero for any point occupied by a particle then an average over the whole system volume becomes $\langle R^2\rangle_V = (1-\phi)\langle R^2\rangle_{\text{empty}}$, so that our replacement for the Carman–Kozeny equation may be written

$$\frac{\mu}{\Gamma} \equiv k \approx 0.6\langle R^2\rangle_V. \tag{21}$$

This, and the other quantities estimated in this section, will be compared with experimental values in section 6, to assess the validity of our model of a sedimenting gel.

5.2. Linear response

In order to obtain the structure's linear response, we shall assume that the rates of formation and breakage are set by thermal excitation. Large and fast imposed deformations of the system would influence these rates, giving rise to a non-linear response. However, we shall restrict our attention to linear response arising from thermal activation. The principal motivation for this is the pursuit of simplicity, in a system of such complexity that the number of parameters required for a detailed description could easily get out of hand. We shall show *a posteriori* that the linear response (and low-frequency) regime is appropriate to at least some of the slowly sedimenting gels investigated. Where the structural viscosity becomes non-linear, we expect it to decrease with applied strain because of a stress-induced increase in the rate of backbone breakage, so that our linear analysis puts an approximate upper bound on the structural viscosity, and therefore on the stress screening length. This is also suggested by experimentally observed shear-thinning of the rheometric shear viscosity at the stresses accessible to rheometry [14], with a non-integer power-law relationship between stress and strain rate. Clearly though, this non-linearity cannot persist to the smallest strain rates, which we believe to be relevant to the early stages of sedimentation since, as calculated below, thermal activation eventually limits the lifetime of elastic elements. In practice, 'shear-thinning' (in this case, compressional thinning) behaviour may be present at the bottom of a sample, where the rate of compression is greatest, while linear response is maintained in the region just above this. So the height to which the compressional 'signal' reaches is still largely determined by the linear response.

5.3. Breakage rate

When thermal activation alone is responsible for structural re-arrangements, the rate-limiting process for breakage of a backbone is the thermal activation of a few load-bearing particles, of radius a, out of several attractive potentials of bond energy U_0. Given that z is the number of bonds required to be broken in order for a load-bearing particle to hop (in fact, roll [18]) from its site on a backbone to a neighbouring site, and that a small number of such rearrangements cause a backbone to yield, dissipating its stored elastic energy, the average lifetime of a backbone, of fractal dimension d_b, is

$$\tau_b \sim \left(\frac{\xi}{2a}\right)^{-d_b} \left(\frac{\Delta^2}{D_0}\right) \frac{\exp(z\beta U_0)}{(z\beta U_0)^2} \tag{22}$$

where $\beta \equiv 1/k_B T$. Here, we have appealed to Arrhenius's law, with a microscopic rate D_0/Δ^2 where D_0 is the diffusion constant of a particle, and Δ is the range of the interaction potential from which it must escape. If, instead of a square well, we assume a ramp potential (which better approximates the depletion potential in a colloid–polymer mixture) then Arrhenius's law becomes modified by the factor $(z\beta U_0)^2$ (from the Smoluchowski equation [24]). The factor $(\xi/2a)^{-d_b}$ is the number of particles in a backbone, and therefore the number of sites at which the backbone could yield [18].

5.4. Healing rate and gelation

When a connection breaks, its associated cluster gains some freedom to move, which it will do until one of its many dangling limbs touches another cluster and forms a new connection, thereby becoming a backbone. Hence, although the unconnected limbs are irrelevant to stress transmission while a cluster's backbone is intact, their geometry controls the rate of 'healing' following the breakage of a connection. This rate of re-connection is limited by the time τ_h taken for a cluster to travel sufficiently far to meet another cluster. In the linear regime,

this motion, unassisted by imposed deformation, is diffusive, with diffusion constant $2aD_0/\xi$. Hence

$$\tau_h \sim R_0^2 \frac{\xi}{2aD_0} \tag{23}$$

where R_0 is the typical distance between clusters.

It is not at all trivial to estimate the inter-cluster distance R_0. Various authors have, explicitly or implicitly, made simplifying assumptions, by setting R_0 equal to the inter-particle spacing in a uniform (not fractally clumped) distribution [18] or equal to the cluster size ξ [25]. The latter assumption is supported by the premise that the percolating structure formed by DLCA is characterized by a single length-scale ξ. In fact, for percolating DLCA aggregates, the clusters of size ξ are separated by sparsely populated, channel-like regions of size $R_0(\gg a)$ whose ratio to ξ, though ϕ independent [23], is small. This length R_0 is closely related to moments of the remoteness distribution (see section 5.1), controlling the value of Γ, the drag coefficient associated with solvent back-flow, since it is the width of the channel of least resistance.

The density of connected, load-bearing clusters will be severely reduced if the time taken for connections to re-form or 'heal' τ_h becomes comparable to or greater than the time between breakages τ_b. In that case, a significant fraction of the clusters will be in a mobile state, not rigidly connected to the percolating network. We shall suggest in section 7 that this is the reason for the eventual collapse of a gel. Initially, however, given that an experimentally observable gel exists, we may assume that this is not the case, so $\tau_b \gg \tau_h$ for a freshly prepared gel. We shall make no further use of the estimate of τ_h, but note that a crude estimate of the gel line could be obtained by solving $\tau_b = \tau_h$ in equations (22) and (23).

5.5. Spring constant

In addition to the rates of breakage and re-connection of a stress-transmitting backbone, we require its spring constant in order to obtain the mechanical response of the network. For a simple spring, the elastic constant k_e is inversely proportional to its length. A load-bearing backbone, however, is a fractal object, so its elastic constant depends on its length ξ via a non-trivial power:

$$k_e = k_0(\xi/2a)^{-Z_c}. \tag{24}$$

In this section we shall find both the 'compliance exponent' Z_c and prefactor k_0.

For a simply connected backbone of fractal dimension d_b, the compliance exponent was calculated by Kantor and Webman [26] as $Z_c \approx 2 + d_b$ in the limit of large ξ. However, lower values of Z_c were measured indirectly, from simulations of two-dimensional aggregates [17], with measured values anywhere from 1.0 to 2.5 ± 0.5 depending on details of the microscopic interactions. The lower values were attributed to the existence of loops in the structures, at the length-scales of fractality ($<\xi$) [17]. We suggest an alternative, though related, explanation.

Firstly notice that the expected result for a simple spring, $Z_c = 1$, is not recovered from Kantor and Webman's result [26] in the limit of a straight chain architecture, $d_b = 1$. This is because their calculation is for a very long random chain, in which compliance is mainly due to bending of its many joints. They explicitly dropped that part arising from stretching, as it grows more slowly with chain length ξ. The result therefore is neither applicable to the simulations of [17] nor to the experimental data [5] analysed in section 6 since, in both cases, the chains are short.

To derive the relevant value of Z_c, we re-visit the calculation of Kantor and Webman [26]. They showed that the elastic energy H due to a force $\boldsymbol{F}$, applied to the end of a chain of N

bonds of undeformed length l between $N+1$ particles at positions $\boldsymbol{R}_i$, is

$$H = \frac{F^2}{2}\left(\frac{NS_\perp^2}{G} + \frac{lL_\parallel}{Q}\right) \tag{25}$$

in terms of constants G and Q associated with local bending and compression respectively. The lengths $S_\perp$ and $L_\parallel$ are given by

$$S_\perp^2 \equiv \frac{1}{NF^2}\sum_{i=0}^{N-1}[\boldsymbol{F}\times(\boldsymbol{R}_N - \boldsymbol{R}_i)]^2,$$

$$L_\parallel \equiv \frac{1}{lF^2}\sum_{i=0}^{N-1}[\boldsymbol{F}\cdot(\boldsymbol{R}_{i+1} - \boldsymbol{R}_i)]^2.$$

It was then shown [26] that $S_\perp$ is of the order of the chain length ξ so that, since $N = (\xi/l)^{d_b}$, the first term of equation (25) implies a force constant

$$k_\perp = \frac{G}{NS_\perp^2} \sim \xi^{-(2+d_b)},$$

yielding the compliance exponent for long chains where this term dominates. For short chains, we now proceed to calculate the compliance exponent from the second term of equation (25). The definition of $L_\parallel$ can be re-written as

$$L_\parallel = lN\,\overline{\cos^2\theta}$$

where the bar indicates an average over all bonds in the chain, and θ is the angle between a bond and the applied force $\boldsymbol{F}$. Note that lN is the contour length of the chain, and that its end-to-end distance is

$$\xi = lN\,\overline{\cos\theta}.$$

Using the Schwartz inequality

$$\overline{\cos\theta} \leqslant \overline{\cos^2\theta} \leqslant 1$$

we deduce

$$1 \leqslant \frac{L_\parallel}{\xi} \leqslant \left(\frac{\xi}{l}\right)^{d_b-1}$$

from which we can put bounds on the elastic constant $k_\parallel$ from the second term of equation (25),

$$\frac{Q}{l^2}\left(\frac{\xi}{l}\right)^{-1} \geqslant k_\parallel \geqslant \frac{Q}{l^2}\left(\frac{\xi}{l}\right)^{-d_b}.$$

Hence, assuming a power-law dependence of the elastic constant on ξ, we find a strong constraint on the compliance exponent

$$1 \leqslant Z_c \leqslant d_b \tag{26}$$

which agrees with expectations for a simple spring when $d_b = 1$.

The constant of proportionality k_0 in equation (24) is the elastic constant on the single-particle scale—a property of the inter-particle potential. For certain interactions, k_0 could be approximated by the second derivative of the potential, but this approximation is inapplicable to singular potentials such as the depletion potential [15]. More precisely, k_0 is a response function, giving the relation between the mean separation $\langle l\rangle$ of a pair of bound particles, and an applied force F, thus $k_0^{-1} \equiv \mathrm{d}\langle l\rangle/\mathrm{d}F$ where $\langle l\rangle = (\mathrm{d}/\mathrm{d}F)\ln\int\exp[-U(l) + Fl]\,\mathrm{d}l$ for an inter-particle potential $U(l)$ in units of k_BT. The range of integration is the range of

the potential, since we consider only bound particles. It follows that the microscopic elastic constant is given by the variance of 'bond lengths', according to $(\beta k_0)^{-1} = \langle l^2 \rangle - \langle l \rangle^2$.

For the experimental system [5], which is a colloid–polymer mixture, the interaction potential is a depletion attraction [15]. For the purpose of order-of-magnitude estimation, we approximate this by a ramp potential of range Δ and depth U_0. Given that $\beta U_0 \gg 1$, the variance of a particle's position in such a potential is $\sim(\Delta/\beta U_0)^2$, so the spring constant of an aggregated backbone is

$$\beta k_e \sim \left(\frac{\beta U_0}{\Delta}\right)^2 \left(\frac{\xi}{2a}\right)^{-Z_c}. \tag{27}$$

5.6. Connection density

In order to estimate the stresses transmitted by the percolating structure, the final quantity we require is the number of load-bearing backbones per unit area, n_b. It has been argued [17, 25] that the distance between percolating backbones defines a different scale from the cluster size ξ observed in density correlations. This is based on the idea that a cluster must move a considerable distance (of order ξ) in order to connect with a neighbour, requiring work to be done to bend some already connected backbones [25]. In fact the nearest points on neighbouring clusters are not separated by ξ, but by a shorter distance, R_0 or less, so that it is relatively easy for each cluster to form connections and carry stress. Indeed, the simulations of sheared gels in [17] support this view, since the 'connectivity length' $n_b^{-1/2}$ is there estimated to be just two or three times the cluster size. Given that we are interested in order-of-magnitude estimates, then, we shall set

$$n_b^{-1/2} \sim \xi \tag{28}$$

which assumes that most clusters transmit stress.

5.7. Structural viscosities

The force transmitted across a unit area in a compressed or sheared network, σ, is simply given by Hooke's law for a number n_b (equation (28)) of appropriately oriented elastic backbones with spring constant k_e (equation (27)), deformed by an amount Δr. That is,

$$\sigma = n_b \, k_e \, \Delta r.$$

Given that a backbone typically has a lifetime τ_b (equation (22)) and length ξ, the typical deformation Δr that it acquires due to a compression rate or shear rate $\dot{\gamma}$ is

$$\Delta r \sim \xi \, \tau_b \, \dot{\gamma}.$$

When, after a time τ_b, a backbone is thermally broken, the elastic energy of deformation that it stored is dissipated. The structural viscosity η (compressional or shear) of the network is defined by $\sigma = \eta\dot{\gamma}$, so we identify

$$\eta \sim n_b \, k_e \, \xi \, \tau_b \tag{29}$$

which, from equations (22), (27) and (28) evaluates to

$$\frac{\eta}{\mu} \sim \left(\frac{2a}{\xi}\right)^{Z_c+d_b+1} \mathrm{e}^{z\beta U_0} \tag{30}$$

where we have used the Stokesian single-particle diffusion constant $D_0 = k_B T/6\pi\mu a$ in a solvent of viscosity μ.

Recall that this structural viscosity is not directly measurable, as it is the viscosity of the particulate network in the absence of its suspending solvent. We have estimated the structural viscosities for compression and shear to be approximately equal, since similar amounts of network deformation occur in either geometry. Hence the screening lengths (r_c, r_s) for compressional and shear stresses, evident in experiments, are expected to be approximately equal. This is despite the very different rheometric responses to compression (which requires compression/expulsion of solvent) and shear (which only requires solvent to be sheared).

6. Comparison with experiments

Let us now summarize our predictions, and compare them with the results of the experiments presented in the companion article [5]. Recall that, in order to estimate the parameters of our continuum model, we have assumed the structure to be that of a fresh gel, i.e. at a short time after formation. Nonetheless, this early-stage physics has implications for the later-stage behaviour.

Firstly, we find qualitative agreement between the theory of section 4 and the experiments reported in the previous article [5]. The experiments showed evidence of a stress screening length in the gels, beyond which momentum transport was not possible. This manifested itself as a characteristic length-scale above which the gel, supported only by backflow of solvent, exhibited a size-independent delay time. Gels smaller than their characteristic length-scale, and thus supported by their interconnected structure, showed size dependence. Both size-dependent and independent delay times were found in the same sample, depending on its size relative to the characteristic length-scale.

We take as a case study the sample, reported in the preceding article [5], with colloidal radius $a = 186$ nm and volume fraction $\phi = 0.200 \pm 0.002$. The polymeric concentration is $C_p = 7.14 \pm 0.14$ mg cm^{-3}. With a polymeric molecular mass $M_w = 320\,000$ g mol^{-1} and radius of gyration $r_g = 17$ nm, this implies an effective colloid–colloid depletion potential of depth $U_0 \approx 6.5 k_B T$ and range $\Delta = 2r_g = 34$ nm.

Our estimate of the drag coefficient Γ (equation (21)) can be compared with experiment if the initial slow sedimentation rate of the gel in the size-independent regime is known. However, in the experimental study [5], no initial settling was observed in the widest samples, due to a very flat meniscus, causing the gelled aggregate to stick to the top solvent–air interface. In the absence of a non-zero measurement of the initial sedimentation rate, we are forced to use the value obtained in the size-dependent regime. We expect the value of v_s in the size-dependent regime to be smaller than the terminal velocity $v_0 = \Delta\rho g \phi_0 / \Gamma$, which allows us to set an upper bound on the drag coefficient Γ. The highest non-zero value of the initial sedimentation rate (in the height-independent regime) is found to be $v_s = 0.03 \pm 0.01\ \mu$m s^{-1}. Using this value, and the density difference of $\Delta\rho = 282$ kg m^{-3} between the colloidal polymethylmethacrylate (PMMA) and the solution of polystyrene in *cis*-decahydronaptheline, we obtain an upper bound on the drag coefficient, $\Gamma \lesssim 1.84 \times 10^{10}$ kg m^{-3} s^{-1}, which we expect to be close to the true value. This is consistent with our theoretical estimate, using equation (21), of $\Gamma \sim 0.8 \times 10^{10}$ kg m^{-3} s^{-1}, providing a second point of agreement between theory and experiment. We have used the viscosity of the polymer solution of $\mu = 3.0 \times 10^{-3}$ Pa s, and $\langle R^2 \rangle_V \approx 0.75\, Q_{\mathrm{gel}}^{-2}$ from simulations [23]. Here, Q_{gel} is the wavenumber at which the structure factor of the fully aggregated system has a peak, and is therefore a measure of the correlation length $\xi \sim 2\pi / Q_{\mathrm{gel}}$. We assume $Q_{\mathrm{gel}} \approx 0.2\, a^{-1}$ [1, 27], which is the value at which Q_{gel} has been reported to saturate for concentrations $\phi \gtrsim 0.1$, and was reported at $\phi = 0.2$ for a colloid–polymer gel very similar to our sample [1].

For this gel [5], a height-dependent delay time was observed, only for initial heights up to 5 mm. Similarly, width dependence was apparent for sample widths around 10 mm and below. We infer that $r_s \sim r_c \sim 5$ mm, confirming a third non-trivial prediction of our theory: due to the similarity of shear and compressional modes of the particle network (though not of the system as a whole) the associated characteristic lengths for a gel sample are approximately equal.

As a fourth 'check-point', we compare the magnitude of the observed characteristic length $r_{c,s} \approx 5$ mm with our theoretical value $r_{c,s} = \sqrt{(\eta/\Gamma)}$, using the estimates of Γ and η in equations (21) and (30). Since the result is very sensitive to the depth of the depletion potential U_0 and to the number z of bonds to be broken in displacing a load-bearing particle, we can expect only order-of-magnitude predictive power, and therefore take the logarithm of the result, yielding

$$\ln \frac{r_{c,s}^2}{\langle R^2 \rangle_V} \approx z\beta U_0 + (Z_c + d_b + 1) \ln \frac{2a}{\xi}. \tag{31}$$

The fractal dimension of the backbone must be a little over unity. Let us use the value for simple percolation [26], $d_b = 1.18$. From equation (26), the compliance exponent then lies in the range $1 \leqslant Z_c \leqslant 1.18$. For definiteness, we use a middle value $Z_c \approx 1.1$. Substituting into equation (31), we obtain the experimentally observed stress transmission length if $z \approx 4$, which, from geometrical intuition, seems an entirely reasonable value, i.e. four bonds must be broken for a particle to leave its load-bearing site, and roll over a pair of neighbours into a non-load-bearing site. Certainly, the orders of magnitude agree.

In our simplified model (equation (10) or (18)), we have made the assumption of a purely viscous network response, neglecting any elastic memory. Our low-frequency, linear analysis is limited by the backbone lifetime to deformation rates below τ_b^{-1}. Rates faster than this will be subject to a non-zero storage modulus (since some backbones remain unbroken) and non-linearity due to stress-affected breakage and healing rates. For our assumptions to be valid, the backbones of the gel structure must break at least once, due to thermal rearrangements, in the time taken for the gel to significantly deform by sedimentation. We must therefore check that the mean breaking time τ_b is less than the time taken for a point in the gel to fall by the characteristic distance r_c at its initial velocity v_0. The ratio of the observed length-scale to early sedimentation speed is $r_{c,s}/v_s = 1.7 \times 10^5$ s $= 46$ h. This is compared with our estimate of the mean lifetime of a backbone (using $z = 4$) from equation (22), $\tau_b = 7 \times 10^4$ s $= 19$ h. Though we do not have the separation of timescales required for our assumption of purely dissipative response to be strictly valid, the fact that $\tau_b < r_{c,s}/v_s$ indicates that corrections due to elasticity would not significantly change our order-of-magnitude calculations. It also validates our picture of a non-solid gel, in which elastic energy is dissipated on experimental timescales. Our estimate of the breaking time τ_b due to thermal rearrangements in equation (22) is sensitive to the value zU_0, so we should remain suspicious of our assumption of linearity. Nonetheless, we have some confidence in our use of a low-frequency (i.e. purely viscous) constitutive relation. We expect that the mean lifetime of structural elements is not very much greater than our estimate, since it would be limited by $r_{c,s}/v_s$ due to stress-induced breakage, leading to shear thinning. This lends weight to our belief (via equation (29)) that the elastic constant of a backbone is not much smaller than our estimate in equation (27). In particular, the experimental data are inconsistent with the values of the compliance exponent calculated in the long-chain limit [26], and with the highest values estimated from simulations of two-dimensional aggregates under shear [17]. Our use of the short-chain limit (see section (5.5)) is further supported by comparing the backbone length ξ to its thickness, which, for tetrahedrally packed particles, is approximately $3.6a$. We obtain $\xi/3.6a \approx 9$, which clearly does not indicate a long chain.

7. Discussion

Transient particulate gels are a poorly understood state of matter, exhibiting varied and often perplexing behaviour. Since much of their underlying physics is unknown, it would be rash to undertake the construction of a quantitatively exact model of these gels. Instead, in this article, we have investigated the broad principles governing their various regimes of behaviour.

Having established that a dissipative coupling between a material with zero yield stress (and well behaved viscosity) and a fixed frame, gives rise to a characteristic length-scale, we have demonstrated that this explains some of the observations of transient gels in colloid–polymer mixtures, reported in the preceding article [5]. The characteristic length-scale is manifested in the saturation of the dependence of gel lifetime on sample height.

Our picture of the transient gel is supported by the observation that the characteristic length-scale associated with the height of a gel sample (due to the compressional mode) is equal to that associated with its width (due to shear), as predicted in section 5. Without our understanding of the mechanics of the gel structure, it would not be immediately obvious that these length-scales should be equal, so the experimental confirmation of the prediction is significant. It is also significant that our calculated estimate of the length-scale is in order-of-magnitude agreement with the measurements.

From our estimate of the drag coefficient, we can further assert that we understand the origin of the initial slow sedimentation rate of the gels in the regime of shallow inter-particle potentials or, equivalently, large containers. Such gels do not have self-supporting structures, but sediment at their terminal velocity, supported predominantly or entirely by drag. These are the samples whose lifetime is independent of the container size. By contrast, gels with inter-particle attractions sufficiently strong that the percolating network can transmit a stress right across the container support some of their own weight as they sediment. These gels collapse at a time that depends on the container size or, in the limit of very strong attractions, have no sudden collapse at all.

Thus, the size dependence of the different behavioural regimes is explained. However, we have not yet accounted for the very existence of a well defined lifetime and a rapid phase of collapse. With our improved understanding of the early stages of sedimentation, let us now speculate on the physics of these phenomena.

As we reasoned in section 3, the collapse must result from a reduction in the network's ability to re-connect or heal itself. A reduction in the healing rate (increase in healing time τ_h) indicates a change in the gel's micro-structure. In particular, from equation (23), since the correlation length ξ is known to vary little between formation and collapse [1], the gap between clusters R_0 must increase.

The ageing and coarsening of the micro-structure of fractal objects is known as sintering. The process can approximate two limiting ideals [28]: sintering by surface diffusion or by viscous flow. In either case, the process is driven by surface tension, which prefers rearrangements that decrease the surface area of an aggregate, thus rounding the corners and smoothing the surface of a crenellated cluster. In the former case, particles cannot move if they are buried within the bulk of a thick backbone or other structural element of the cluster, so that the only mobile particles are those in the surface layer, which can diffuse by hopping across the surface of the aggregate. These particles tend to diffuse away from highly curved regions such as the tips of the finest feathery tendrils, causing such fingers to withdraw and the void between clusters to increase in width R_0. In the latter case, sintering by viscous flow, particles buried inside the treelike branches are not frozen, but can re-arrange with a finite viscosity. Thus when the finest tendrils are withdrawn, their material is not only re-distributed over the surface of the aggregate, but flows in bulk through its branches and backbones. In a numerical

study [28], it was shown that the two processes have very dissimilar consequences for the large-scale evolution of isolated clusters. The diameter (i.e. largest linear dimension) of such a cluster undergoing viscous flow was shown to shrink continuously from the onset of sintering, varying with time t approximately as t^{1-2/d_f} in two dimensions. In contrast, surface diffusion was observed to coarsen the structure on the smallest length-scales first, and to proceed through a hierarchy of lengths, while the overall diameter of the isolated cluster remains approximately constant until the very late stages [28]. In either case, if sintering clusters are not isolated (as in the cited numerics [28]) but aggregated (as in the gels), the withdrawal of the finest protrusions should result in an increase of R_0 and, by equation (23), a reduction in the healing rate. In simple terms, with fewer outstretched fingers, a falling cluster is not so quickly caught by its neighbours. This coarsening, then, is the cause of the ultimate failure of the transient gel.

The colloidal PMMA particles used in the experiments [5] behave as almost ideal hard spheres. Light scattering data on similar samples to those discussed in this paper [3] show a peak in the structure factor at a wavenumber corresponding approximately to one particle diameter, thus indicating that, locally, particles are closely packed within the structure of the aggregates. At random close packing, hard spheres behave as a glass, with local caging of particles leading to a large (possibly divergent) viscosity. Further evidence for glassy behaviour in the gels, in the form of the dynamic structure factor, comes from dynamic light scattering experiments [3]. In the light of this, we do not expect particles buried within an aggregated branch, and surrounded by their full complement of close-packed neighbours, to have any significant mobility, compared with those at a free surface. It therefore appears most likely that ageing of our aggregates of hard colloids proceeds by surface diffusion sintering.

By contrast, it is interesting to note that ageing of a transient gel was recently observed in experiments on a colloidal suspension of polystyrene in water [29]. The polystyrene particles were sufficiently soft to be easily deformed by interactions, and could even fuse together[4]. Despite the absence of gravitational compaction, since the particles were made neutrally buoyant by tuning the proportions of H_2O and D_2O in the solvent, the gelled aggregates were observed to shrink continuously throughout the experiment [29]. It seems reasonable to interpret these observations as indicating sintering of the soft particulate aggregates by viscous flow, as opposed to the surface diffusion process expected with hard particles. We note that the bond strengths (by Van der Waals attraction) in those experiments [29] were much higher than in our own, so that momentum would propagate over distances far in excess of the sample size, and elastic response was dominant on experimental timescales.

Having considered the coarsening process (surface diffusion) and its driving force (surface tension), it remains only to discuss the rate at which the sintering occurs. This depends on the mechanism by which particles are activated to hop between sites on the aggregate surface. In section 5 we assumed this was by thermal Brownian motion within the binding potential, and inferred the resulting structural viscosity of the freshly formed network. In the later stages of collapse, large-scale hydrodynamic motions are clearly visible to the naked eye [3, 5]. In the gels with fairly weak inter-particle attractions, colloidal material torn from the aggregate can be seen to be expelled 'volcanically' into the supernatant from the top surface of the collapsing gel. It is clear then that, at some point in the gel's development, back-flow of solvent becomes a dominant influence on the rearrangement of particles.

It is not a trivial task to model the activation of surface diffusion by the solvent flow field, but we can speculate on certain aspects of the process. If the sintering rate is a function of the speed of solvent back-flow and not entirely dominated by thermal activation as we expect in the

[4] The fusion of particles was described in [29] as 'sintering'. This is a different usage of the word from that applied in this paper. We use it to mean a coarsening of the entire fractal cluster, due to rearrangements of its constituent particles, as also interpreted in [28].

early stages, then clearly it is an increasing function. The sintering causes the gaps or channels between clusters to widen and so, from equation (21), the drag coefficient Γ decreases. We can consider this flow-activated surface diffusion sintering to be akin to the erosion process that forms rivers. If the gel sample is much smaller than its characteristic stress transmission length, then the non-buoyant weight of the network ($\boldsymbol{f}$ in equation (1), or the LHS of equation (10)) is predominantly supported structurally, and a decrease in the drag coefficient is irrelevant to the sedimentation rate. If, on the other hand, the characteristic length is small compared with the container, then the aggregate's weight is supported predominantly by drag ($\Gamma \boldsymbol{v}$), so a decrease in Γ results in an increase in the sedimentation speed v to maintain force balance. Since the sintering rate is an increasing function of the speed of solvent back-flow, and therefore of v, we have a positive feedback loop, leading to a runaway sedimentation speed. We therefore expect to see a signature of positive feedback in those samples with such weak interactions that $r_{c,s}$ is small compared with the container, and no such signature for very strong or small samples. The sudden collapse evident in the experiments [5] is just such a signature, and is absent from the strongest and shortest gels, for which our estimate of $r_{c,s}$ exceeds the sample dimensions, and in which 'creeping' behaviour [5] is observed. We note, however, that, by the time the sedimentation rate becomes strongly non-linear, highly complex hydrodynamics are apparent in the experiments [5]. Such phenomena are beyond the scope of our model, which is valid only for the early stages, though it is during the early stages that the subsequent fate of the gel is fixed.

8. Conclusion

In summary, transient gelation is a non-classical, though ubiquitous, phase-ordering phenomenon. Though several studies have probed the early stages of gelation [1–3], transient gels remain poorly understood, particularly in the later stages, when they collapse by delayed sedimentation. Though we have not attempted to calculate the delay time for the regime where collapse is sudden, we have identified the factors on which it depends.

While a gel is still freshly formed, the structure of its particulate network is tenuous, with only small intervening cavities of solvent. Since this structure suppresses large-scale hydrodynamics, we have been able to construct a model where solvent dynamics are summarized in a dissipative coupling of the particulate network to a fixed (non-Galilean-invariant) frame. We have shown that such a coupling, in the absence of zero-frequency elasticity, results in a novel class of matter, 'torpid matter', which will not transmit momentum beyond a finite distance. We have demonstrated that the colloid–polymer transient gels reported in the accompanying experimental article [5] are an example of this peculiar matter, by identifying the characteristic length-scale (in both compressional and shear modes), and establishing order-of-magnitude agreement with the predicted size. We have further shown how a sample's behaviour is controlled by the ratios of its width, height and stress-transmission length. Along the way, we have derived new, useful formulae for the permeability of fractal porous media, and for the elasticity of a short fractal strut (the opposite limit to that previously calculated [26]).

In order to understand better the mechanisms of collapse, we suggest that the influence of solvent flow on the erosive sintering of fractal objects would be a fruitful area of study.

Acknowledgments

Our thanks go to Michael Cates, Wilson Poon, Steve Meeker and Margaret Robins for helpful discussions. RMLE acknowledges the support of the Royal Society of Edinburgh (SOEID fellowship), and LS is grateful for the help of the Institute of Food Research.

References

[1] Poon W C K, Pirie A D and Pusey P N 1995 *Faraday Discuss.* **101** 65
[2] Grant M C and Russel W B 1993 *Phys. Rev.* E **47** 2606
[3] Poon W C K, Starrs L, Meeker S P, Moussaïd A, Evans R M L, Pusey P N and Robins M M 1999 *Faraday Discuss.* **112** 143
[4] Soga K G, Melrose J R and Ball R C 1998 *J. Chem. Phys.* **108** 6026
[5] Starrs L, Poon W C K, Hibberd D J and Robins M M 2002 *J. Phys.: Condens. Matter* **14** 2485
[6] Chaikin P M and Lubensky T C 1995 *Principles of Condensed Matter Physics* (Cambridge: Cambridge University Press)
Bray A J 1994 *Adv. Phys.* **43** 357
[7] Vicsek T 1992 *Fractal Growth Phenomena* 2nd edn (Singapore: World Scientific)
[8] Haw M D, Sievewright M, Poon W C K and Pusey P N 1995 *Adv. Colloid Interface Sci.* **62** 1
[9] Hobbie E K 1997 *Phys. Rev.* E **55** 6281
Hobbie E K 1999 *Langmuir* **15** 8807
[10] Bergenholtz J and Fuchs M 1999 *Phys. Rev.* E **59** 5706
Bergenholtz J, Fuchs M and Voigtmann Th 2000 *J. Phys.: Condens. Matter* **12** 6576
[11] Allain C, Cloitre M and Wafra M 1995 *Phys. Rev. Lett.* **74** 1478
[12] Glasrud G G, Naverrete R C, Scriven L E and Macoskco M C 1993 *AIChE J.* **39** 560
[13] Robins M M, Kim Ng, Gunning P A and Parker A 1995 *Int. Proc. ACS Symp.*
[14] Meeker S P 1997 *Edinburgh University Thesis*
[15] Asakura S and Oosawa F 1954 *J. Chem. Phys.* **22** 1255
Asakura S and Oosawa F 1958 *J. Polym. Sci.* **33** 183
[16] See, e.g., the two-fluid model of viscoelastic phase separation,
Tanaka H 2000 *J. Phys.: Condens. Matter* **12** R297
However, that model relies on knowledge of a free energy, which cannot easily be defined for a non-ergodic particulate gel, and results in spongelike textures that are not observed in the present system.
[17] West A H L, Melrose J R and Ball R C 1994 *Phys. Rev.* E **49** 4237
[18] Potanin A A, De Rooij R, Van den Ende D and Mellema J 1995 *J. Chem. Phys.* **102** 5845
[19] Darcy H P G 1856 *Les Fontaines Publiques de la Ville de Dijon* (Paris: Dalmont)
[20] Heijs A W J and Lowe C P 1995 *Phys. Rev.* E **51** 4346
[21] Schwartz L M, Martys N, Bentz D P, Garboczi E J and Torquato S 1993 *Phys. Rev.* E **48** 4584
[22] Carman P C 1937 *Trans. Inst. Chem. Eng.* **15** 1550
[23] Evans R M L and Haw M D, in preparation (cond-mat/0202202)
[24] Hänggi P, Talkner P and Borkovec M 1990 *Rev. Mod. Phys.* **62** 251
[25] Wessel R and Ball R C 1992 *Phys. Rev.* A **46** R3008
[26] Kantor Y and Webman I 1984 *Phys. Rev.* E **52** 1891
[27] Bibette J, Mason T G, Hu Gang and Weitz D A 1992 *Phys. Rev. Lett.* **69** 981
[28] Olivi-Tran N, Thouy R and Jullien R 1996 *J. Physique* I **6** 557
[29] Cipelletti L, Manley S, Ball R C and Weitz D A 2000 *Phys. Rev. Lett.* **84** 2275